Effect of Periodic Disinfection on Persisters in a One-Dimensional Biofilm Model

Cogan, NG, Szomolay, B & Dindos, M. 2013, 'Effect of Periodic Disinfection on Persisters in a One-Dimensional Biofilm Model', Bulletin of Mathematical Biology, Vol. 75, No. 1, pp. 94-123

Effect of Periodic Disinfection on Persisters in a One-Dimensional Biofilm Model

N. G. Cogan[1] ***Barbara Szomolay***[2]***, Martin Dindos***[3]

Department of Mathematics, Florida State University[1]
Mathematics Institute, University of Warwick[2]
Maxwell Institute for Mathematical Sciences, The University of Edinburgh[3]

Abstract

It is well known that disinfection methods that successfully kill suspended bacterial populations often fail to eliminate bacterial biofilms. One focus of recent efforts to understand biofilm survival has been on the existence of small, but very tolerant, subsets of the bacterial population termed persisters. In this investigation we analyze a mathematical model of disinfection that consists of a susceptible-persister population system embedded within a growing domain. This system is coupled to a reaction-diffusion system governing the antibiotic and nutrient. Previous mathematical models either neglected the spatial aspect of the biofilm, or were explored computationally. Here, we have analyzed the effect of periodic and continuous dosing protocols on persisters in a one-dimensional biofilm model, both analytically and numerically.

We provide sufficient conditions for the existence of steady-state solutions and numerically show that non-uniqueness may occur. Our results indicate that for large periods it is more effective to apply the antibiotic for a higher percentage of the period. For shorter periods this may not be as effective. In addition, we computationally studied the effectiveness of periodic dosing compared to continuous dosing as a function of the length of period and the fraction of period devoted to dosing, assuming either that the average antibiotic dose is constant, or, that the applied dose during on-time is constant.

1 Introduction

Bacterial biofilms arise in a wide variety of natural, industrial and medical environments [1–3]. In many situations biofilms are sources of recalcitrant infections and impurities; therefore it is often the goal to eliminate the biofilm using biocides or antibiotics. However, the biofilm lifestyle provides a wide range of protective mechanisms for the bacteria that exist within the biofilm [4, 5]. Understanding the protection mechanisms and predicting novel disinfection protocols can be done experimentally or mathematically. In this manuscript we extend previous mathematical studies that focus on physical, physiological and phenotypic mechanisms [6–9] and focus on the effects of periodic disinfection of a spatially extended model that includes an extremely tolerant sub-population of the bacteria, termed persisters.

The material properties of the biofilm and the dynamics of the deformation response to the bulk fluid motion has been shown to have an effect on the survival of the bacteria [10], although this response is most likely overwhelmed by other tolerance mechanisms [11], so we limit the mechanics in this study to the simplest response, namely erosion. The current study includes three main tolerance mechanisms that are known to play a role in bacterial persistence: physical, physiological and phenotypic tolerance.

Physical protection arises because of the polymeric gel that surrounds and binds the bacteria. Biofilms do not behave as well-mixed populations and the disinfectant reaches the bacteria via diffusion [12–14]. Therefore the thickness of the biofilm plays a role in the dynamics of the disinfectant since the concentration is governed by reaction/diffusion processes. The concentration of biocide is also influenced by advection, but this does not play a role in this investigation.

For antimicrobials that target the reproduction cycles of the bacteria (e.g. antibiotics), respiration plays an important role [5]. It is well known that most antibiotics are more effective in killing actively reproducing bacteria [15]. At the same time, it is well known that most bacteria within the biofilm are in nutrient depleted regions with the layers nearer to the bulk flow actively growing (since they have access to the nutrient source within the bulk flow) and consuming the nutrient before it can reach deeper within the biofilm [16]. In this way, bacteria in the nutrient depleted zones are protected from disinfection while growing slower than the more susceptible, faster growing surface layers.

We note that physiological protection is transient. If antimicrobials are constantly applied, the surface layers will be killed allowing nutrient to penetrate further leading the killing of bacteria deeper within the biofilm. This is in stark contrast to most observations of biofilms that indicate that biofilms are refractory to constant disinfectant challenges [17]. Even though many bacteria are killed, not all bacteria are susceptible. These observations have lead to a variety of hypotheses regarding the persistence of small fractions of the population. The two dominant hypotheses are adaptive responses and persister formation. Each of these argues that bacteria alter their activity in response to antimicrobial challenge, although in different ways.

Adaptive response describes the process of bacterial populations altering their metabolism in response to low levels of antimicrobial challenge. That is, before the antimicrobial concentration reaches a lethal level, some cells transition into an adapted state that renders them tolerant to higher level challenge. Because the spatial heterogeneity of the biofilm induces chemical gradients and hinders the penetration of chemicals, bacteria deep within the biofilm may have sufficient time at sub-minimal concentration to react to the challenge [18]. A mathematical model described in [19,20] incorporates these assumptions into a spatially extended, partial differential equation (PDE) model of the bacteria dynamics within a one dimensional, flat slab biofilm. One of the main results in [19] is that for small doses of antimicrobials on-off dosing is always more effective than constant dosing and that biofilm thickness is important for effective dosing. Indeed, at low dosage levels thin biofilms are better treated with a single dose per period which is in line with experimental studies. Moreover, refractory treatment (where a second application of biocide is *less* successful than the initial challenge) is also observed for both thin and thick biofilms. While biologically distinct from adaptive responses, the phenomenon of persister cells leads to models that are mathematically related to those in [19,20] and suggest the utility of on-off type dosing protocols.

The persister cell hypothesis is well described by Lewis *et al.*, suggesting that persister cells are also distinct physiologically from susceptible cells [21, 22]. However, instead of a transition *into* the protected stated that depends on the challenge concentration, it is the transition *out of* the persistent state that is dose dependent. In particular, when bacteria grown in planktonic environments (or from disrupted biofilm [23]) are taken at discrete time intervals and exposed to high concentrations of antibiotic, a fraction of the popula-

tion survives the challenge. The fraction depends on the growth stage of the planktonic cells. Further, persisters seem to survive extremely long challenges without reversion to the susceptible state until the challenge is removed. This motivates a novel disinfection strategy: by periodically applying antibiotic, the entire population might be killed. The first challenge kills the susceptible cells, leaving persister cells. Withdrawing the antibiotic allows the persister cells to begin to revert to susceptible cells. By timing the periodic application, these susceptible cells can be killed again before the population has full recovered. This hypothesis has been tested mathematically in several papers, with varying level of details and the optimal protocol has been established [6–8, 10]. We note that this concept has not been explored fully experimentally. The only published experimental results that we are aware of focus on bacterial infection in patients with Cystic Fibrosis [24]. Interestingly, the authors find that after long-term, periodic applications of antibiotics, there is accumulation of mutants that produce persisters at a higher rate. We do not include this mechanism in the present investigation, but it should be noted that there was no investigation into the *optimal* timing in these experiments. As we show below, there is window of timing were periodic disinfection is the optimal protocol. It is quite easy to find periodic regimes that are not successful. Thus we argue that it is vital to understand the dynamics of the population to determine the optimal disinfection.

The purpose and scope of the current study is to consider analytic and computational results for periodic disinfection of a one dimensional biofilm model. Here we study the problem in one-dimension in order to obtain both analytic and computational results for the optimal timing of the disinfection cycle. The analytic studies are important since the particular computational results rely on estimating certain parameters while the analytic results are much more general. We argue that the qualitative features of our results – namely that there is a window of periods/dose fractions where alternating disinfection is the optimal protocol. This study also explores the effects of the dosing period and dose/withdrawal ratio more fully than has been done before.

The manuscript is organized as follows: We first describe the mathematical model that governs the bacterial population (susceptible, persister and dead), nutrient and biocide concentrations and the dynamic thickness of the biofilm. We then describe the analytic results that have been obtained for the model including the steady-state analysis and predictions regarding periodic disinfection. The analytic results are complemented with numerical simulations that deal with the non-uniqueness of steady-states and consider varying dose frequency, period, application method and key parameters. We then collect the results into an extended conclusion/discussion section.

2 The biofilm model

We assume that the bacterial population consists of three phenotypes: susceptible cells volume fraction, B_s, persister cells volume fraction, B_p, and dead susceptible cells volume fraction, B_{sd}. We consider only one growth-limiting substrate, C, and assume that biomass constituents are incompressible. The biofilm is treated as a continuum that is fully saturated and the fluid component is neglected; therefore $B_s + B_p + B_{sd} = 1$. The spatial domain is $x \in [0, L(t)]$, the equations governing the cell volume fractions are obtained from conservation of mass (which is equivalent to conservation of volume if the

densities are constant [25]:

$$\frac{\partial B_s}{\partial t} + \underbrace{\frac{\partial}{\partial x}(vB_s)}_{\text{advection}} = \underbrace{g(C)B_s}_{\text{growth}} - \underbrace{k_d A g(C) B_s}_{\text{disinfection}} - \underbrace{k_l g(C) B_s}_{\text{loss}} + \underbrace{k_r(A) B_p}_{\text{gain}} \tag{1}$$

$$\frac{\partial B_{sd}}{\partial t} + \frac{\partial}{\partial x}(vB_{sd}) = k_d A g(C) B_s \tag{2}$$

$$\frac{\partial B_p}{\partial t} + \frac{\partial}{\partial x}(vB_p) = k_l g(C) B_s - \underbrace{k_r(A) B_p}_{\text{reversion}}, \tag{3}$$

where $x = 0$ represents the impermeable substratum the biofilm is attached to and $x = L$ represents the biofilm-bulk fluid interface. The dynamics of bacterial species is driven by the growth-induced advective velocity, v, which is determined by the incompressibility constraint. The population of susceptible cells in (1) changes due to growth, death due to killing with antibiotic, A, loss due to transition to persister cells and gain as persister cells revert back to susceptible cells. Note that in the case of persisters, reversion is often assumed in the absence of antibiotics [8, 21]. More generally, it is reasonable to take

$$k_r(A) = \begin{cases} k_r^0 & \text{if } A = 0 \\ k_r^1 & \text{if } A > 0, \end{cases}$$

where $k_r^0 \gg k_r^1 \geq 0$. The population of persister cells in Equation (3) changes due to the net gain of transition between susceptible and persister cells. The dead cell population in Equation (2) increases due to disinfection of susceptible cells. Our model is a one-dimensional counterpart of the chemostat model of ODEs in [8] (with zero wash-out rate). The reduction of Equations (1)-(3) to ODEs along characteristics $s(t) \in (0, M]$ for some $M > 0$ gives the aforementioned ODE system in [8]. Unlike the persister model in [8], we also consider the dynamics of the antibiotic concentration.

While biologically different from the tolerance of persisters to antibiotics, the theory of adaptive resistance leads to models that are mathematically related to equations (1)-(3) (see [19]- [20], where a mathematical model of bacterial adaptation without substrate limitation, i.e., with saturation, has been analyzed). A notable difference between the two biofilm defense mechanisms is that adapted cells grow at a growth rate comparable to that of the susceptible ones, whereas the population of persister cells only changes due to conversion to and from susceptible cells. Moreover, in case of adaptation, the adapted-susceptible cell reversion rate is independent of the presence of antibiotics.

We suppose that the living and dead cells react with the antibiotic at the same rate (i.e., we have a reactive antimicrobial such as β-lactam antibiotics) and that the substrate is being consumed only by the susceptible population. Hence, the antibiotic and the substrate concentration in dimensional variables will satisfy the equations

$$\frac{\partial A}{\partial t} = D_a \frac{\partial^2 A}{\partial x^2} - kA$$

$$\frac{\partial C}{\partial t} = D_c \frac{\partial^2 C}{\partial x^2} - f(C) B_s,$$

where D_a, D_c are the diffusion rates and k is the antibiotic-cell reaction rate. Diffusion limitation arises in biofilms because fluid flow is reduced and the diffusion distance is

increased with biofilm thickness. The relative effective diffusivity is expressed as the ratio D_e/D_{aq}, where D_e, D_{aq} are the diffusion coefficients of the solute in biofilms and water, respectively, and are usually on the order of $10^{-6} - 10^{-5}\text{cm}^2\text{s}^{-1}$. For example, the value of D_e/D_{aq} is ca. 0.6 for light gases (e.g., oxygen, methane) and ca. 0.25 for most organic solutes [12]. For antibiotics, the values of these diffusion coefficients have been estimated in [13].

The time scale for biofilm penetration is on the order of minutes. This is much shorter than the duration of antibiotic exposure, which is typically tens of hours [14]. Hence, it can be assumed that the antibiotic and substrate concentration is quasi-static, i.e, the time derivatives $\frac{\partial A}{\partial t}, \frac{\partial C}{\partial t}$ can be neglected. If l is a characteristic biofilm thickness and τ is a typical treatment time, then this assumption means that the characteristic times for antibiotic and substrate diffusion ($l^2 D_a^{-1}$ and $l^2 D_c^{-1}$) are small compared to the treatment time τ and the other time scales ($1/k_d, 1/k_l, 1/k_r^0$).

Following other one-dimensional biofilm models [19], [20], the biofilm thickness $L(t)$ changes in response to advection and detachment of biomass, where the detachment process is taken as an erosion, i.e., removal of small groups of cells from the surface of the biofilm. Unlike sloughing (detachment of large particles of biomass), erosion can be viewed as a continuous process occurring uniformly over the surface of the biofilm [26]. Several models for detachment have been proposed in the literature [26], [27]. Our detachment model assumes a first-order dependence on the biomass constituents, second-order dependence on the biofilm thickness and the same detachment rate coefficient for the living and dead cells. The advective velocity v is obtained by summing equations (1)-(3) and taking into account the incompressibility condition. Finally, the dimensionless model equations are

$$\frac{\partial^2 A}{\partial x^2} = \phi_a^2 A \tag{4}$$

$$\frac{\partial^2 C}{\partial x^2} = f(C) B_s \tag{5}$$

$$\frac{\partial B_s}{\partial t} + \frac{\partial}{\partial x}(v B_s) = (1 - k_d A - k_l) g(C) B_s + k_r(A) B_p \tag{6}$$

$$\frac{\partial B_{sd}}{\partial t} + \frac{\partial}{\partial x}(v B_{sd}) = k_d A g(C) B_s \tag{7}$$

$$\frac{\partial B_p}{\partial t} + \frac{\partial}{\partial x}(v B_p) = k_l g(C) B_s - k_r(A) B_p \tag{8}$$

$$\frac{\partial v}{\partial x} = g(C) B_s \tag{9}$$

$$\frac{dL}{dt} = v(L,t) - \sigma L^2, \tag{10}$$

where the function f is assumed to be nonnegative, locally Lipschitz continuous satisfying $f(0) = 0$ and the function g is locally Lipschitz continuous, nondecreasing and positive for positive values. Typically Monod kinetics are assumed and in this manuscript we specify the functions f, g to be $f(C) = \frac{\beta C}{C + K_S}$ and $g(C) = \frac{\alpha C}{C + K_S}$.

We note that the dimensionless parameter ϕ_a called Thiele modulus compares the rates of antibiotic-cell reaction and diffusion (see [19], [26]). When ϕ_a is small, diffusion is small compared to reaction and the antibiotic penetrates well. On the other hand, when ϕ_a is

large ($\gg 1$), the biofilm is never fully penetrated by the antibiotic. With larger reaction rates, ϕ_a can attain values of the order of magnitude of 10 [26].

The boundary conditions associated with (4)-(10) are

$$\begin{aligned}
&\frac{\partial A}{\partial x}(0,t) = 0, \quad A(L(t),t) = u(t) \ \text{ for } \ 0 \le t \le P \\
&\frac{\partial C}{\partial x}(0,t) = 0, \quad C(L(t),t) = K \ \text{ for } \ 0 \le t \le P \\
&v(0,t) = 0 \ \text{ for } \ 0 \le t \le P,
\end{aligned} \tag{11}$$

where $u(t)$, the externally applied antibiotic concentration, is a nonnegative piecewise continuous function of period P, and $K > 0$ is the externally applied substrate concentration. It readily follows from (9) and (11) that

$$A(x,t) = u(t)\frac{\cosh(\phi_a x)}{\cosh(\phi_a L(t))}. \tag{12}$$

To explore optimal dosing strategies, we associate the problem (4)-(11) with functionals to be minimized with respect to the externally applied antibiotic concentration $u(t)$. Antibiotics can be bactericidal (killing bacteria, e.g., β-lactam antibiotics) and bacteriostatic (inhibiting the growth of bacteria giving the immune system time to mount lethal response to the bacteria, e.g. tetracycline). As in [19], we introduce two types of functionals: functional J (the long-term average of the number of living cells) and functional J_L (the long-term average of biofilm thickness). We note that our parameter choices are given in Table I.

Numerical simulations suggest that given any initial data, the solution of the problem (4)-(11) becomes periodic as $t \to \infty$ with period P. Hence, we can define the functionals

$$\begin{aligned}
J(u) &= \lim_{T\to\infty} \frac{1}{P}\int_T^{T+P}\int_0^{L(t)} (B_s(x,t) + B_p(x,t))dxdt, \\
J_L(u) &= \lim_{T\to\infty} \frac{1}{P}\int_T^{T+P} L(t)dt.
\end{aligned} \tag{13}$$

Note that all parameters will be dimensionless in the throughout this paper. We make estimates for the ratios $\max(k_r(.))/\alpha$, $\max(k_r(.))/k_d$, α/σ and α/k_l based on [19] and [7]. In particular, we take $k_r^0/\alpha = 0.01 - 1$ and $k_r^0/k_d = 5 - 10$ for on-off dosing, but for constant dosing, when k_r^0 is replaced by k_r^1, these ratios are much smaller. Also, we take $\alpha/\sigma = 5 - 10$ and $\alpha/k_l = 100 - 500$.

3 Steady-state solutions

If the externally applied antibiotics concentration is constant, the solutions of equations (6)-(10) are expected to converge to a steady-state solution. In this section we study all possible steady-state solutions of our system. The stationary system will be reduced to a 2D non-autonomous system, which will in turn allow us to determine sufficient conditions for the existence of trivial/non-trivial steady-states. A biofilm model of adaptive resistance has been analytically studied in [19] - we will later draw comparisons between the steady-state analysis results obtained here and in [19].

The steady-state equations corresponding to equations (6)-(10) are

$$\frac{d}{dx}(vB_s) = g(C)B_s(1 - k_dA - k_l) + k_r(A)B_p \tag{14}$$

$$\frac{d}{dx}(vB_{sd}) = k_dAg(C) \tag{15}$$

$$\frac{d}{dx}(vB_p) = k_lg(C)B_s - k_r(A)B_p \tag{16}$$

$$\frac{dv}{dx} = g(C)B_s, \tag{17}$$

with

$$A(x) = u_0\frac{\cosh(\phi_a x)}{\cosh(\phi_a L)} \tag{18}$$

for $0 \leq x \leq L$, where L is the steady-state biofilm thickness, u_0 is the constant antibiotics concentration applied through the interface and C solves (5). The corresponding boundary conditions are

$$v(0) = 0, \quad v(L) = \sigma L^2, \quad \frac{dC}{dx}(0) = 0, \quad C(L) = K. \tag{19}$$

Since B_{sd} is uniquely determined by B_s, we can restrict ourselves to a system of two equations with unknowns B_s, B_p satisfying the ODEs

$$\frac{dB_s}{dx}v = g(C)B_s(1 - k_dA - k_l - B_s) + k_r(A)B_p \tag{20}$$

$$\frac{dB_p}{dx}v = g(C)B_s(k_l - B_p) - k_r(A)B_p. \tag{21}$$

The re-parametrization by characteristics has been used earlier for a similar model [] and we are going to use it again. The equation of characteristics corresponding to (20)-(21) reads

$$\frac{ds}{dt} = v(s(t)), \quad v(0) = L, \tag{22}$$

where the parameter t is chosen such that range of the function $s(t)$ is $(0, L]$ or a subset of it. We note that Eq. (22) has a C^1-solution on $(-\infty, 0]$ and that this statement is also true when there are only dead cells remaining deep in the biofilm, i.e., $B_s + B_p = 0$ on $[0, x_0]$ for some $0 \leq x_0 \leq L$ (for details see [20]).

From now on we will use the re-parametrization of the steady-state solutions B_s, B_p, C and A. Define

$$b_s(t) := B_s(s(t)), \quad b_p(t) := B_p(s(t)), \quad c(t) := C(s(t)), \quad a(t) := A(s(t)).$$

Then, by Eq. (20)-(21), the functions b_s, b_p satisfy the non-autonomous system

$$\frac{db_s}{dt} = g(c(t))b_s(1 - k_da(a) - k_l - b_s) + k_r(a(t))b_p \tag{23}$$

$$\frac{db_p}{dt} = g(c(t))b_s(k_l - b_p) - k_r(a(t))b_p. \tag{24}$$

System (23)-(24) does not depend on v and by the continuity of s, a, and c we have $a(t) \to A_0$ and $c(t) \to C_0$ as $t \to -\infty$, where $A_0 = A(x_0), C_0 = C(x_0)$. Hence, in the limit $t \to -\infty$ the non-autonomous system (23)-(24) can be approximated by an autonomous ODE system (25)-(26) that we study next.

3.1 Autonomous system

We consider the autonomous system

$$\frac{db_s}{dt} = g(C_0)b_s(1 - k_d A_0 - k_l - b_s) + k_r(A_0)b_p \tag{25}$$

$$\frac{db_p}{dt} = g(C_0)b_s(k_l - b_p) - k_r(A_0)b_p, \tag{26}$$

where A_0, C_0 are defined in Section 3. One can show that the range of solutions for the system (25)-(26) is a triangle in the first quadrant given by

$$\Delta = \{(b_s, b_p) \in \mathbb{R}^2 : \quad b_s, b_p \geq 0, \quad b_s + b_p \leq 1\}$$

and that Δ is a positively invariant region.

Obviously, the autonomous system always has a trivial equilibrium and possibly a non-trivial one that we show in the Lemma below.

Lemma 1. *Denote $m := 1 - k_d A_0$. Let $k_r(A_0) > 0$. For $m > 0$, the autonomous system (25)-(26) has a non-trivial equilibrium in the region Δ. If $m \leq 0$ the only equilibrium in Δ is $(0, 0)$.*

If $k_r(A_0) = 0$, all points on the line $\{(0, t);\, t \in [0, 1]\}$ are equilibria. In addition, if $m > k_l$, the point $(m - k_l, k_l)$ is also an equilibrium.

Proof. The steady-state solutions corresponding to Eq. (25)-(26) satisfy

$$b_s g(C_0)(m - k_l - b_s) + k_r(A_0)b_p = 0$$
$$b_s g(C_0)(k_l - b_p) - k_r(A_0)b_p = 0,$$

from which follows that $m = b_s + b_p$ and

$$b_s = \frac{g(C_0)(m - k_l) - k_r(A_0) + \sqrt{D}}{2g(C_0)}, \quad b_p = \frac{g(C_0)(m + k_l) + k_r(A_0) - \sqrt{D}}{2g(C_0)}, \tag{27}$$

where

$$D = (g(C_0)(m - k_l) - k_r(A_0))^2 + 4g(C_0)mk_r(A_0). \tag{28}$$

(We will later use the notation (b_s^e, b_p^e) to refer to the coordinates of the non-trivial equilibrium.)

We obtain that the coordinates of the non-trivial equilibrium given in (27) are both non-negative if

$$\frac{|\sqrt{D} - g(C_0)k_l - k_r(A_0)|}{2g(C_0)} \leq \frac{m}{2}. \tag{29}$$

It can be shown that the inequality in (29) is true for $m \geq 0$. Hence, the claim follows. If $k_r(A_0) = 0$ it follows immediately from the equations that $b_s = 0$ guarantees that a given point is an equilibrium. □

The following statements deal with the stability of the trivial/non-trivial equilibria.

Lemma 2. *If $k_r(A_0) > 0$, for $m < 0$, the trivial equilibrium is a sink, otherwise, for $m > 0$, the trivial equilibrium is a saddle point. If $k_r(A_0) = 0$, then the trivial equilibrium is not an isolated fixed point.*

Proof. If A is matrix of linearization corresponding to the autonomous system (25)-(26) about $(0, 0)$, then the characteristic matrix $A - \lambda I$ becomes

$$\mathbf{A} - \lambda\mathbf{I} = \begin{pmatrix} g(C_0)(m - k_l) - \lambda & k_r(A_0) \\ g(C_0)k_l & -k_r(A_0) - \lambda \end{pmatrix}.$$

Hence, the eigenvalues are determined by the formula

$$\lambda_{1,2} = \frac{g(C_0)(m - k_l) - k_r(A_0) \pm \sqrt{D}}{2},$$

where D is given by (28). From this the claim follows. □

Lemma 3. *If $k_r(A_0) > 0$ and $m > 0$, then the non-trivial equilibrium (b_s^e, b_p^e) given by (27) is a sink. If $k_r(A_0) = 0$ and $m - k_l > 0$, the point $(m - k_l, k_l)$ is a stable node.*

Proof. If A^ϵ is matrix of linearization corresponding to the autonomous system (25)-(26) about (b_s^e, b_p^e), then the characteristic matrix $A - \lambda^\epsilon I$ becomes

$$\mathbf{A}^\epsilon - \lambda^\epsilon\mathbf{I} = \begin{pmatrix} g(C_0)(m - k_l - 2b_s^e) - \lambda & k_r(A_0) \\ g(C_0)k_l & -k_r(A_0) - g(C_0)b_s^e - \lambda \end{pmatrix}.$$

Considering that $b_s^e + b_p^e = m$, we can show that the eigenvalues satisfy

$$\lambda_{1,2}^e + g(C_0)b_s^e = \frac{g(C_0)(b_p^e - k_l) - k_r(A_0) \pm \sqrt{D^e}}{2},$$

where $D^e = (g(C_0)(b_p^e - k_l) - k_r(A_0))^2 + 4g(C_0)k_r(A_0)(m - b_s^e) \geq 0$. We will show that the trace and determinant of A^ϵ are $Tr(A^\epsilon) < 0$ and $det(A^\epsilon) > 0$, which proves the claim.

We have $Tr(A^\epsilon) = g(C_0)(m - k_l - 3b_s^e) - k_r(A_0)$. Taking the formula for b_s^e from (27) implies that the condition $Tr(A^e) < 0$ is equivalent to

$$0 < g(C_0)(m - k_l) - k_r(A_0) + 3\sqrt{D},$$

where D is given by (28). This shows that $Tr(A^e) < 0$.

We also have $det(A^e) = -g(C_0)(m - k_l - 2b_s^e)(k_r(A_0) + g(C_0)b_s^e) - k_r(A_0)g(C_0)k_l$. Again, taking the formula for b_s^e from (27) gives

$$\begin{aligned} det(A^e) &= \frac{1}{2}\Big[D - k_r(A_0)^2 + \sqrt{D}g(C_0)(m - k_l) - k_r(A_0)g(C_0)(m + k_l)\Big] \\ &= \frac{g(C_0)}{2}\Big[g(C_0)(m - k_l)^2 + k_r(A_0)(m + k_l) + \sqrt{D}(m - k_l)\Big]. \end{aligned} \tag{30}$$

It could be shown that (30) is positive for all $m > 0$.

If $k_r(A_0) = 0$ and $m - l_l > 0$, then the eigenvalues are $\lambda_1 = \lambda_2 = -g(C_0)(m - k_l) < 0$ which corresponds to a stable node. □

It follows that whenever (0,0) is a saddle point, there is a nontrivial equilibrium. Now, it follows from the characteristic matrix $A - \lambda I$ that the eigenvectors of the characteristic

matrix could be taken

$$\Big(1, \frac{-g(C_0)(m-k_l) - k_r(A_0) \pm \sqrt{D}}{2k_r(A_0)}\Big). \tag{31}$$

If $(0,0)$ is a saddle point ($\lambda_1 > 0, \lambda_2 < 0$), it could be shown that the sign of the coordinates of the eigenvectors is $(+,+)$ for λ_1 and $(+,-)$ for λ_2.

Define the line corresponding to λ_1

$$l_{13} = \Big((b_s, b_p) : b_p = \frac{-g(C_0)(m-k_l) - k_r(A_0) + \sqrt{D}}{2k_r(A_0)} b_s\Big).$$

We will show that l_{13} going through the first and third quadrant is an unstable invariant manifold. As a consequence we will have that the line corresponding to λ_2

$$l_{24} = \Big((b_s, b_p) : b_p = \frac{-g(C_0)(m-k_l) - k_r(A_0) - \sqrt{D}}{2k_r(A_0)} b_s\Big)$$

going through the second and fourth quadrant is a stable invariant manifold.

Lemma 4. *The line l_{13} is an invariant manifold, i.e., if $(b_s(0), b_p(0)) \in l_{13}$, then $(b_s(t), b_p(t)) \in l_{13}$ for all t. Moreover, if $m > 0$, the coordinates of the non-trivial equilibrium (b_s^e, b_p^e) lie on the line segment $l_+ = l_{13} \bigcap \Delta$.*

Proof. If the coordinates of $(b_s, b_p) \in l_{13}$, then they satisfy

$$\begin{aligned}
&(g(C_0)(m-k_l-\lambda)b_s + k_r(A_0)b_p = 0\\
&g(C_0)k_l b_s - (k_r(A_0)+\lambda)b_p = 0,
\end{aligned}$$

where λ is the eigenvalue of the characteristic matrix $A - \lambda I$. Hence,

$$\frac{db_s}{db_p} = \frac{db_s}{dt}\Big(\frac{db_p}{db_t}\Big)^{-1} = \frac{\lambda b_s - g(C_0)b_s^2}{-g(C_0)b_s b_p + \lambda b_p} = \frac{2k_r(A_0)}{-g(C_0)(m-k_l) - k_r(A_0) + \sqrt{D}} = \frac{b_s}{b_p} \tag{32}$$

for any $(b_s, b_p) \neq (0,0) \in l_{13}$ and this is what we wanted. The statement that $(b_s^e, b_p^e) \in l+$ could be shown algebraically. □

We will show below that if $(0,0)$ is the only equilibrium, it is globally asymptotically stable, and if there are two equilibria, then (b_s^e, b_p^e) given by (27) is globally asymptotically stable.

Lemma 5. *If $m < 0$ and $k_r(A_0) > 0$, the trivial equilibrium is globally asymptotically stable.*

Proof. We will show that for any point $X = (b_s, b_p) \in \Delta$ the ω-limit set of the autonomous system (25)-(26) is $\omega(X) = (0,0)$. Obviously, $\omega(X)$ is connected and nonempty. Since the triangular domain Δ is compact and positively invariant, it contains either a limit cycle, or an equilibrium point. We can exclude $\omega(X)$ being a limit cycle, since in this case, by the Poincare-Bendixon Theorem $\omega(X)$ would be a periodic orbit. Inside the loop of a periodic orbit there must be an equilibrium point, i.e., we would have $(0,0)$. However, part of the loop would be outside Δ which is not possible. Hence, $\omega(X) = (0,0)$ and this proves the claim. □

Lemma 6. *If $m > 0$ and $k_r(A_0) > 0$, the nontrivial equilibrium is globally asymptotically stable.*

Proof. Consider the ω-limit set of the system (25)-(26) for any point $X = (b_s, b_p) \in \Delta \setminus \{(0,0)\}$. First we will show that $\omega(X) \neq (0,0)$. Since the trivial equilibrium is an unstable saddle point ($\lambda_1 > 0, \lambda_2 < 0$), there exists a stable manifold given by the line l_{24} going through the second and fourth quadrant which is outside the triangular region Δ. Hence, any solution starting inside Δ will not converge to $(0,0)$ as $t \to \infty$.

We are left to show that $\omega(X) = (b_s^e, b_p^e)$. By the same argument as in Lemma 4, $\omega(X)$ is either a limit cycle or the nontrivial equilibrium. If $\omega(X)$ was a limit cycle, again by the Poincare-Bendixon Theorem $\omega(X)$ would be a periodic orbit with (b_s^e, b_p^e) inside its loop. However, the nontrivial equilibrium also lies on the line segment l_+ and hence, the loop around (b_s^e, b_p^e) would intersect l_+ in at least two points, which is contradiction with the uniqueness of solutions. Hence, the proof is complete. □

3.2 Existence of steady-state solutions

We observe first that the system (4)-(10) always has a steady-state solution such that $L = 0$. The question is whether there is a steady-state solution for $L > 0$. We shall answer this in two steps. Initially we will ignore the equation (10) for L and assume that $L > 0$ is given to us. We have the following two results:

Theorem 1. *Suppose that $L > 0$ is given and*

$$m = 1 - k_d A(0) > 0, \qquad \text{where: } A(0) = u_0/\cosh(\phi_a L). \tag{33}$$

Then there exists at least one continuous nonzero steady-state solution of the system (4)-(10) satisfying boundary conditions (11).

Conversely, for given $L > 0$ if (B_s, B_p, C, v) is a continuous nonzero steady-state solution of the system (4)-(10) on the interval $[0, L]$ satisfying boundary conditions (11), then (B_s, B_p, C, v) solves the ODE system

$$\begin{aligned}
\frac{dB_s}{dx} &= \frac{1}{v}\left[g(C)B_s(1 - k_d A - k_l - B_s) + k_r(A)B_p\right], \\
\frac{dB_p}{dx} &= \frac{1}{v}\left[g(C)B_s(k_l - B_p) - k_r(A)B_p\right], \\
\frac{d^2C}{dx^2} &= f(C)B_s, \\
\frac{dv}{dx} &= g(C)B_s,
\end{aligned} \tag{34}$$

on the interval $[0, L]$ with initial conditions:

$$B_s(0) = b_s, \quad B_p(0) = b_p, \quad C(0) = C_0, \quad \frac{dC}{dx}(0) = 0, \quad v(0) = 0. \tag{35}$$

Here C_0 is a number from the interval $(0, K]$ and (b_s, b_p) is the nontrivial equilibrium shown to exist in Lemma 1 given by (27).

Theorem 2. *Suppose that $L > 0$ is given and*

$$m = 1 - k_d A(0) \leq 0, \qquad \text{where: } A(0) = u_0/\cosh(\phi_a L). \tag{36}$$

Then the only continuous steady-state solution of the system (4)-(10) satisfies $B_s = B_p = 0$ on $[0, L]$.

Proof of Theorem 1. We have to overcome the issue that C solves a second order equation on $[0, L]$ and depends on B_p, hence we cannot solve it as easily as the equation for A whose solution is $A(x) = u_0 \cosh(\phi_a x)/\cosh(\phi_a L)$. We deal with this issue by considering the ODE system (34) $[0, L]$ with initial conditions (35).

Here the initial condition for the nutrient, C_0 (which will be chosen later), is any number from the interval $(0, K]$ and (b_s, b_p) is the nontrivial equilibrium given by (27). We want to show that there is a value C_0 such that $C(L) = K$, for that value of C_0 the solution of the ODE system (34) is also a steady state solution of (4)-(10) satisfying boundary conditions (11).

The solvability of the system (34) with initial conditions (35) follows from standard ODE theory provided $v > 0$ (to avoid the case $1/v$ being undefined). This unfortunately is the case at $x = 0$. To deal with this let us write $B_s(x)$ and $B_p(x)$ near $x = 0$ as

$$B_s(x) = b_s + O(x), \qquad B_p(x) = b_p + O(x). \tag{37}$$

If follows that $v(x) = g(C_0)b_s x + o(x)$, hence if g is positive for nonzero values of C_0 we see that $v(x) = O(x)$. Now writing

$$g(C)B_s(1 - k_d A - k_l - B_s) + k_r(A)B_p = O(x), \tag{38}$$

due to cancellations as (b_s, b_p) is the equilibrium. Hence

$$\frac{dB_s}{dx} = \frac{1}{v}\left[g(C)B_s(1 - k_d A - k_l - B_s) + k_r(A)B_p\right] = O(1),$$

with similar statement holding for $\frac{dB_p}{dx}$ near $x = 0$. This implies that the ODE system (34) is regular even at $x = 0$, hence the standard solvability theory applies on the whole interval $[0, L]$. From this we get that the system (34) with initial conditions (35) has a unique solution on $[0, L]$ for any $C_0 > 0$.

Consider now a map $F : C_0 \mapsto C_{C_0}(L)$ where $C_{C_0}(x)$ is the solution of (34) - (35) where $C_{C_0}(0) = C_0$. We claim that due to continuous dependence of solvability of (34) on initial conditions F is continuous. Also note that if $C_0 \to 0+$ then $F(C_0) \to 0+$ (see equation (4) and the assumption that $f(0) = 0$). Finally $F(C_0) \geq C_0$ as $C'' \geq 0$ and $C'(0) = 0$. Hence by the intermediate value theorem there is at least one value $C_0 \in (0, K]$ such that $F(C_0) = K$. For this value, the system (34) - (35) is the non-zero steady-state solution of (4)-(10) satisfying boundary conditions (11).

For the converse, if (B_s, B_p, C, v) is a continuous nonzero steady-state solution of the system (4)-(10), then it must satisfy (34) on the interval $(0, L]$. Also obviously in the boundary conditions (11) we have that $v(0) = 0$, $C'(0) = 0$ and $C(0) \in (0, K]$. We only have to establish that $(B_s(0), B_p(0))$ must equal to (b_s, b_p) given by (27).

To see this we recall the re-parametrization $s : (-\infty, 0] \to (0, L]$ introduced above that turns equations (34) for B_s and B_p into non-autonomous system (23)-(24) where

$b_s(t) := B_s(s(t))$, $b_p(t) := B_p(s(t))$. We want to understand the behavior of $(b_s(t), b_p(t))$ as $t \to -\infty$. Recall, that α-limit set of a solution is the set of all accumulations points of the solution as $t \to -\infty$. As $(b_s(t), b_p(t)) \in \Delta$ the α-limit set of this solution is a nonempty subset of Δ. Notice also that as $t \to -\infty$ the system (23)-(24) approaches the autonomous system (25)-(26). Thus the α-limit set of the solution $(b_s(t), b_p(t))$ is either an equilibrium or a limit cycle of the autonomous system (25)-(26). However, we have shown that (25)-(26) has no limit cycle and only two equilibria: $(0, 0)$ and (b_s, b_p) given by (27). Thus either

$$B_s(0) = \lim_{t \to -\infty} b_s(t) = 0, \qquad B_p(0) = \lim_{t \to -\infty} b_p(t) = 0,$$

or

$$B_s(0) = b_s, \qquad B_p(0) = b_p.$$

To finish our proof we have to show the the first option does not happen. We will prove this by contradiction, let us assume that indeed $\lim_{t \to -\infty} b_s(t) = \lim_{t \to -\infty} b_p(t) = 0$. Recall also that $\frac{ds}{dt} = v(s(t))$, hence

$$L = L - 0 = s(0) - s(-\infty) = \int_{-\infty}^{0} v(s(t))\, dt.$$

Since v is monotone nondecreasing it follows that $w(t) = v(s(t)) \to 0$ as $t \to -\infty$. Hence by the ODE v satisfies we see that

$$\frac{dw}{dt} = \frac{dv}{ds}\frac{ds}{dt} = g(C(s(t)))B_s(s(t))v(s(t)) = g(C(s(t)))b_s(t)w(t).$$

Hence

$$\frac{d}{dt}(\ln w) = \frac{1}{w}\frac{dw}{dt} = g(C(s(t)))b_s(t) \le g(K)b_s(t),$$

since g is a monotone function. It follows that

$$\ln w(0) - \ln w(-T) \le g(K) \int_{-T}^{0} b_s(t)\, dt,$$

for all $T > 0$. Since $w(0) = v(L)$ and $w(-T) \to 0$ as $T \to \infty$ we get that

$$\int_{-\infty}^{0} b_s(t)\, dt = \infty.$$

Recall that we do know how solutions $b_s(t)$ will look near 0. The equilibrium at $(0, 0)$ has one positive eigenvalue $\lambda > 0$, hence we get that near this point

$$\frac{db_s}{dt} = \lambda b_s + o(b_s),$$

i.e., $\frac{d}{dt}(\ln b_s) = \lambda + o(1)$, hence

$$b_s(-T) = b_s(0) \exp[-(\lambda + o(1))T], \qquad \text{as } T \to \infty.$$

This means that the integral $\int_{-\infty}^{0} b_s(t)\, dt$ is finite which is a contradiction. □

Proof of Theorem 2. The argument is similar as the one given above. Assume that there is a continuous nonzero steady-state solution of the system (4)-(10). Again, consider the re-parametrization $s : (-\infty, 0] \to (0, L]$ introduced above that turns equations (34) for B_s and B_p into non-autonomous system (23)-(24). By same argument as given above, if we consider the α-limit set of the solution $(b_s(t), b_p(t))$ on $(-\infty, 0]$ then this set will consist of equilibria and limit cycles of the autonomous system (25)-(26). Given the assumption $m \leq 0$ the only equilibrium is $(0, 0)$ and there is no limit cycle. Hence $b_s(t), b_u(t) \to 0$ as $t \to -\infty$. We claim that this implies that $b_s(t) = b_u(t) = 0$ for all $t \leq 0$ (hence $B_s = B_p = 0$ on $[0, L]$) from which the claim of Theorem 2 follows.

Indeed, assume that this is false. Then $b_s(t) + b_u(t) > 0$ for $t < 0$ and $b_s(t), b_u(t) \to 0$ as $t \to -\infty$. This is however impossible. For a fixed large nonnegative t we have that

$$m(t) = 1 - k_d A(t) < 1 - k_d A(0) \leq 0,$$

which implies that $(0, 0)$ is an equilibrium with two negative eigenvalues. Since we looking at the limit $t \to -\infty$ we are reversing time. In the reverse time $(0, 0)$ is therefore totally unstable and $(b_s(t), b_u(t))$ cannot approach zero but has to move away from it as $t \to -\infty$. Hence the only option is that $b_s(t) = b_u(t) = 0$ for all $t \leq 0$. □

In the previous two theorems we have ignored the steady state equation for L, namely that $v(L) = \sigma L^2$ and instead we have assumed that L is given. We shall prove now that the existence (and non-existence) of continuous nonvanishing steady-state solution of the full system (4)-(10) satisfying boundary conditions (11) depends on the size of u_0, for small values there is such solution, on the other hand for large values of u_0 the only continuous steady state solution has $L = 0$.

Theorem 3. *Assume that the parameters ϕ_a, ϕ_c, α, k_r, k_d, k_l, K, $\sigma > 0$ and the function f (monotone nondecreasing, continuous and nonzero for positive values) are given and fixed.*

Then there exist a value u^1 such that for all $u_0 \in [0, u^1)$ there is at least one continuous nonzero steady state solution of the system (4)-(10) satisfying boundary conditions (11). Moreover, we have an estimate:

$$u^1 \geq \frac{1}{k_d}.$$

On the other hand, there exists a value $u^2 \geq u^1$ such that for all $u_0 \geq u^2$ the only continuous steady state solution of the system (4)-(10) satisfying boundary conditions (11) has length zero, i.e., $L = 0$. Moreover we have an estimate:

$$u^2 \leq \frac{\cosh(\phi_a g(K)/\sigma)}{k_d}.$$

Remark. Realistically, we expect $u^1 = u^2$ however in order to do that we would have to establish that for all $u_0 \in [u^1, u^2)$ there is a nonzero steady state solution. We, however, lack the monotonicity of the map $u_0 \mapsto C_0(u_0)$, where C_0 is the value of the function C at zero. It might happen then that for some u in this interval this map is not monotone, and hence, it might be possible to have $u^1 < u^2$. We have not observed such situation in our simulations, but this scenario cannot be excluded.

Proof. We start by dealing with the nonexistence result. Let us assume first that $u_0 \geq \frac{\cosh(\phi_a g(K)/\sigma)}{k_d}$. By contradiction let us assume that there is a nonzero steady-state solution

of the system (4)-(10) satisfying boundary conditions (11) of positive length $L > 0$. Then $L \leq L_{max} = g(K)/\sigma$, since

$$v(L) \leq g(K)L, \qquad \text{hence:} \quad 0 = v(L) - \sigma L^2 \leq L(g(K) - \sigma L).$$

Clearly for $L > g(K)/\sigma$ the right-hand side is negative so the upper bound on L must hold. It follows that

$$A(0) = \frac{u_0}{\cosh(\phi_a L)} \geq \frac{u_0}{\cosh(\phi_a L_{max})} = \frac{u_0}{\cosh(\phi_a g(K)/\sigma)}.$$

Hence,

$$m = 1 - k_d A(0) \leq 1 - k_d \frac{u_0}{\cosh(\phi_a g(K)/\sigma)} \leq 0.$$

From this by Theorem 2 we have that $B_s = B_p = 0$ on $[0, L]$, so $v(L) = 0$ and hence $0 = v(L) - \sigma L^2 = -\sigma L^2$. From this $L = 0$. It follows that if we define

$$\begin{aligned} u^2 = \inf\{z \geq 0; \quad & \text{if } u_0 \geq z \text{ then (4)-(10) with boundary conditions (11)} \\ & \text{has no continuous steady state of nonzero length}\}, \end{aligned} \tag{39}$$

then

$$u^2 \leq \frac{\cosh(\phi_a g(K)/\sigma)}{k_d}.$$

Now, define

$$\begin{aligned} u^1 = \sup\{z \geq 0; \quad & \text{if } 0 \leq u_0 < z \text{ then (4)-(10) with boundary conditions (11)} \\ & \text{has a continuous steady state of nonzero length}\}. \end{aligned} \tag{40}$$

Clearly $u^1 \leq u^2$. If we prove that for any $u_0 < \frac{1}{k_d}$ there is a non-zero steady state of positive length then the whole claim is established.

Once again, any such steady-state solution has to satisfy $L \leq L_{max} = g(K)/\sigma$ by the same argument as given above. This gives a lower bound on the value of $C(0) = C_0$ since it follows that any C that solves (4) on $[0, L]$ has a subsolution c defined on $[0, L_{max}]$ by

$$\frac{\partial^2 c}{\partial x^2} = \left(\sup_{x \in [0,K]} \frac{f(x)}{x} \right) c, \quad c'(0) = 0,\, c(L_{max}) = K.$$

Here, the supremum of $f(x)/x$ exists as we assume that $f(0) = 0$ and f is Lipschitz on $[0, K]$. Hence always $C \geq c$ on $[0, L]$ so we see that we only have to consider $C_0 \in [c(0), K]$ (and $c(0) > 0$ provided $K > 0$).

It also follows by our assumption that

$$A(0) = \frac{u_0}{\cosh(\phi_a L)} \leq u_0 < \frac{1}{k_d},$$

hence

$$m = 1 - k_d A(0) > 0$$

and Theorem 1 applies.

Consider a map $F : [c(0), K] \times [0, L_{max}] \to \mathbb{R}^2$ defined as follows. For each pair (C_0, L) we consider the unique solution (B_s, B_p, C, v) of the ODE system (34) with initial conditions (35) and A given by (18) on $[0, L]$. Here (b_s, b_p) is the nontrivial equilibrium given by (27). We define

$$F(C_0, L) = (C(L) - K, v(L) - \sigma L^2).$$

By continuous dependence of solutions of ODE on its initial condition we get that F is a continuous function of two variables C_0 and L. We now want to restrict the domain of F to a smaller box $[c(0), K] \times [L_{min}, L_{max}]$ where $L_{min} > 0$ is chosen as follows:

$$F_2(C_0, L_{min}) = v(L_{min}) - \sigma L_{min}^2 \geq \varepsilon > 0, \quad \text{for some } \varepsilon > 0 \text{ and all } C(0) \in [c(0), K].$$

Here F_2 is the second component of the map $F = (F_1, F_2)$. Such value L_{min} exists because

$$\frac{\partial F_2}{\partial L}(., 0) \geq \delta > 0, \quad \text{and} \quad F_2(., 0) = 0.$$

Indeed, $\frac{\partial F_2}{\partial L}(., 0) = g(C_0)B_s(0) \geq g(c(0)) \inf b_s$. Here $g(c(0)) > 0$ and the infimum is taken over all b_s given by (27) for $C(0) \in [c(0), K]$. Due to our assumptions $\inf b_s > 0$.

The question is whether for some pair (C_0, L) in the domain $D = [c(0), K] \times [L_{min}, L_{max}]$ of the map F we have $F(C_0, L) = (0, 0)$, as for such pair the solution (B_s, B_p, C, v) of the ODE system (34) with initial conditions (35) is a nonzero steady-state solution of the system (4)-(10) satisfying boundary conditions (11).

We know that at the boundary ∂D of our domain we have:

$$F_2(., L_{min}) > 0, \quad F_2(., L_{max}) \leq 0, \quad F_1(c(0), .) \leq 0, \quad F_1(K, .) \geq 0. \tag{41}$$

Hence we either have $(0, 0) \in F(\partial D)$ and we are done or

$$\deg(F, (0, 0)) = -1.$$

This can be seen from (41) as the image of the ∂D is a closed curve $F(\partial D)$ that loops once around $(0, 0)$ and has orientation reverse to ∂D. Hence as $\deg(F, (0, 0)) \neq 0$ it follows that $(0, 0) \in F(D)$. This establishes existence of nonzero steady-state solution for all $u_0 < 1/k_d$. □

3.3 Uniqueness/Non-uniqueness of steady-state solutions

Theorem 3 does not exclude the possibility that for given $u_0 \in [0, u^1)$ there is more than one solution - as exemplified by numerical simulations (Figures 1-4). Due to substrate limitation we cannot make statements about the uniqueness of steady-states even for small antibiotic doses. However, the bifurcation diagram shown in Figure 2 indicates that for large antibiotic doses there may be non-unique solutions. This is similar to results obtained for models of bacterial adaptation in [19] and [20]. The latter paper deals with saturating substrate kinetics. A similar mechanism is at work in case of substrate-limitation, when an appropriate initial dose can influence dosing efficacy. That is, the time dependent solution $L(t)$ may converge to different steady-states depending on the initial dose of antibiotic (Figure 3). From the proof of Theorem 3 it follows that the nullsets of the map F will

determine the non-trivial steady-states of the system (4)-(10). As Figure 4 shows, multiple solutions are possible.

Figure 1. For given $u_0 = 9.68$, the function $v(L) - \sigma L^2$ has been plotted for $0 \leq L \leq 5$. There are three intersection points with the x-axis (Figure 1 (a)). This becomes obvious when zooming in the neighborhood of $L = 0$ in Figure 1 (b).

Figure 2. To further explore the solutions L of the equation $v(L) - \sigma L^2 = 0$, they have been plotted as the function of u_0. The lower estimate of u^1 from Theorem 3 is $k_d^{-1} = 10$ in this example, whereas $u^1 = u^2 \approx 25.8$. A vertical line in close proximity to $u_0 = 10$ intersects the curve at three different points, hence, there are three different solutions of L (with two being stable). For example, as in Figure 1, for $u_0 = 9.68$, there are two stable solutions, $L = 0.2$ and $L = 4.6$. For $10 < u < u^1$, there are two solutions, with one being stable.

Figure 3. Two stable solutions of L are also possible in the case of substrate limitation. When antibiotic dose of $u_0 = 50$ is added on the time interval $[0, 25)$ and $u_0 = 100$ is added otherwise, the biofilm thickness would converge to $L = 0$ (Figure 3 (a)). However, a smaller initial dose would affect the biofilm thickness by converging to the larger value $L = 1.2$ (Figure 3 (b)).

Figure 4. As shown in Theorem 3, the nullsets of the map $F(C_0, L) = (C(L) - K, v(L) - \sigma L^2)$ determine the solutions (B_s, B_p, C, v) of (34), and hence, the nontrivial equilibria of the system (4)-(10). For given L and $C(0) = c_0$, the solutions of the equations $C(L) = K$ and $v(L) = \sigma L^2$ are plotted for different values of σ. For small detachment rates only trivial steady-state exists (Figure 4 (a)), however, as σ is increased, even three intersection points of the nullsets are possible, in which case there are two stable solutions (Figure 4 (c)).

As a final remark we add that as in the case of adaptation [20], uniqueness of steady-states can be shown for small doses of antibiotic in the saturated case. Indeed, when no antibiotic is given ($u_0 = 0$), the steady-state solutions satisfy $B_s = \frac{\alpha(1-k_l)-k_r^0+\sqrt{D}}{2\alpha}$ and $L = \frac{\alpha B_s}{\sigma}$, where $D = (\alpha(1 - k_l) - k_r^0)^2 + 4\alpha k_r^0$. The argument goes then as in [20].

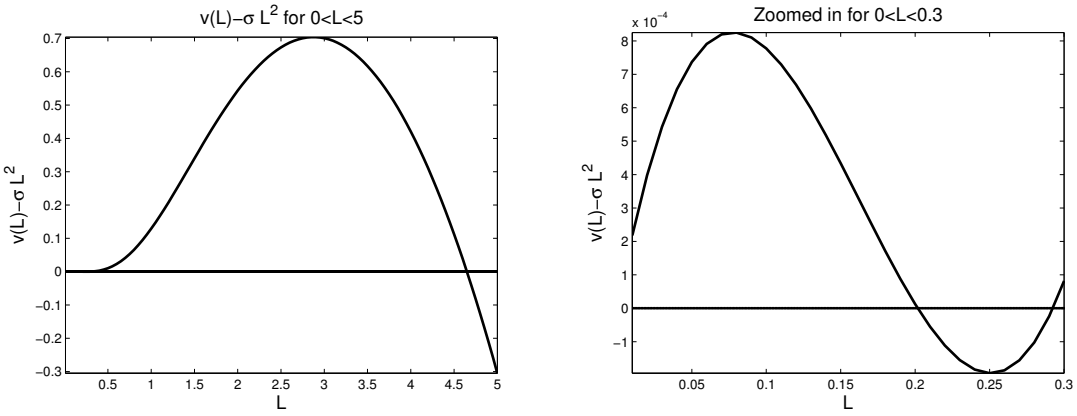

(a) (b)

Figure 1: We show the function $v(L) - \sigma L^2$ (i.e. the difference between erosion and the interface velocity) for the case of substrate saturation. We find three intersections. The left panel shows intersection near zero and one larger intersection. The right panel shows that there are two intersections at small thicknesses. The parameters are: $\alpha = 1, u_0 = 9.68, \phi = 1, k_d = 0.1, k_l = 0.01, k_r^1 = 0.005, \sigma = 0.2$

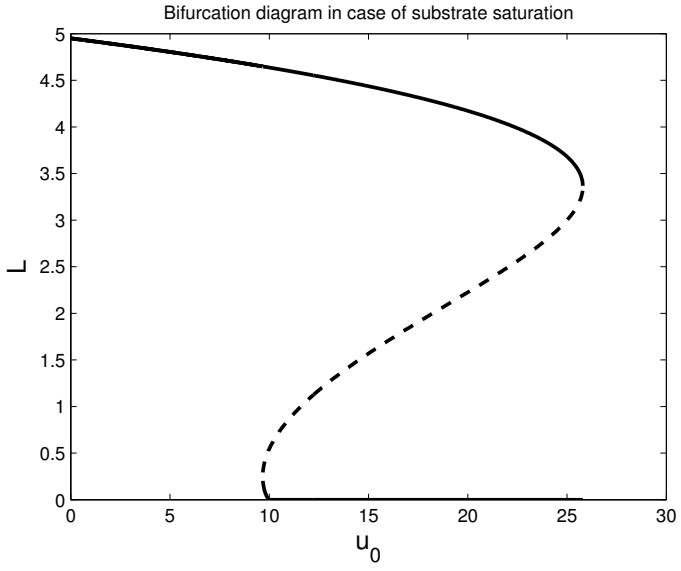

Figure 2: We show the bifurcation diagram, using u_0 as the bifurcation parameter, for the case of substrate saturation. Here the parameters are: $\alpha = 1, \phi = 1, k_d = 0.1, k_l = 0.01, k_r^1 = 0.005, \sigma = 0.2$

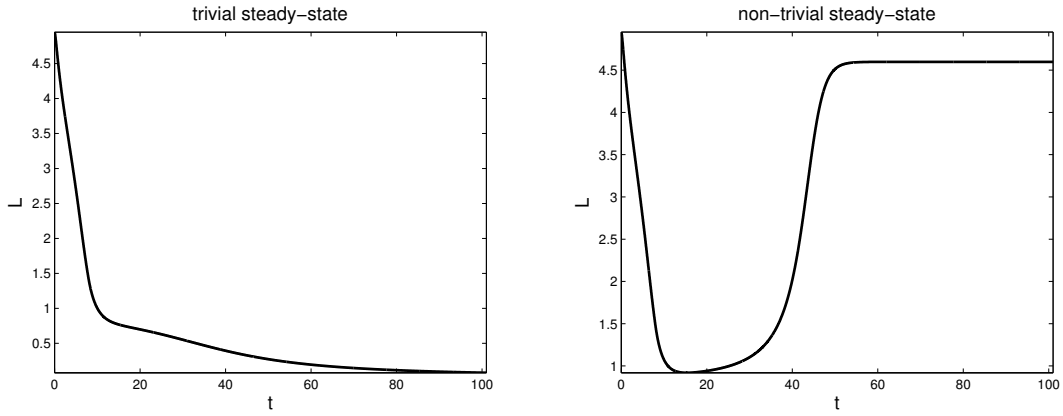

(a) (b)

Figure 3: We show the dynamics of the steady-state for different parameter sets. This numerical results complements the analytic observation of the existence of two stable steady-states (one positive and one zero). Depending on the disinfection, either may be achieved. The parameters are: $\alpha = 1, \phi = 1, k_d = 0.1, k_l = 0.01, k_r^1 = 0, \sigma = 0.2, K = 1, K_S = 1, \beta = 1$ a) $u_0 = 50$ for $0 \leq t < 25$ and $u_0 = 100$ for $t \geq 25$ b) $u_0 = 8$ for $0 \leq t < 25$ and $u_0 = 100$ for $t \geq 25$

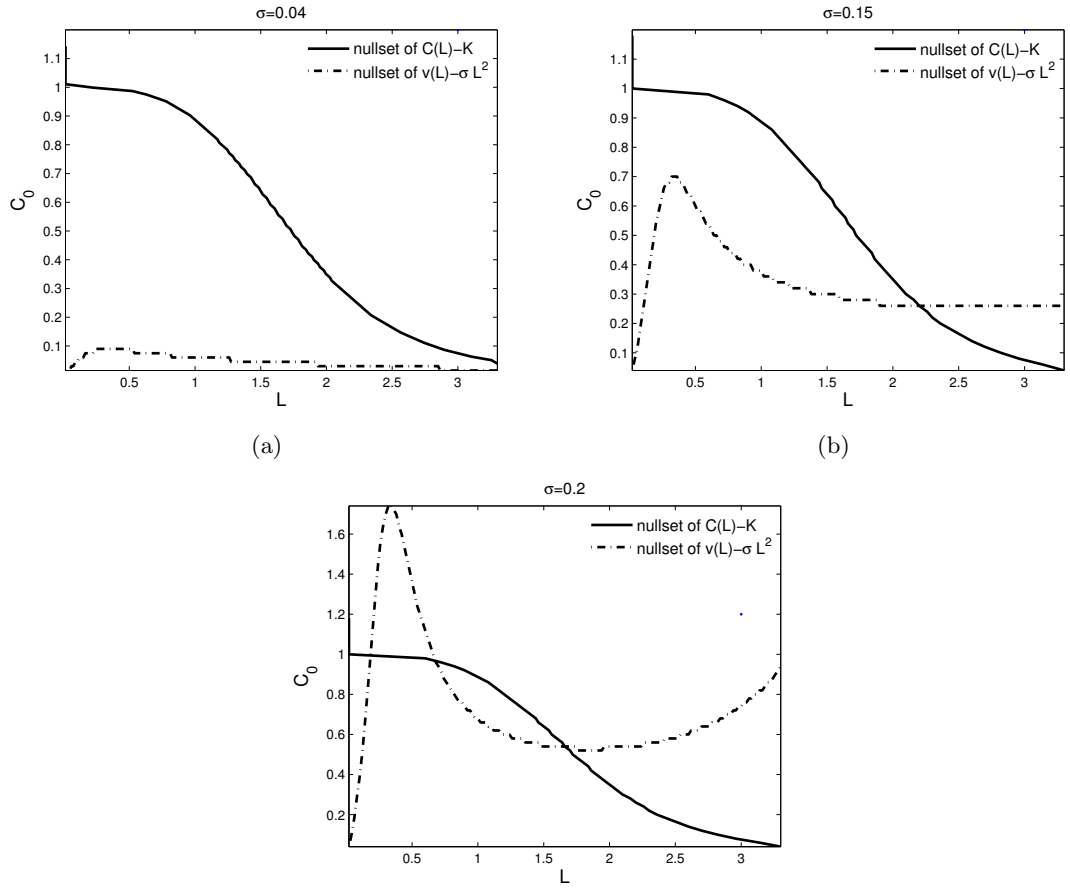

Figure 4: We show the nullsets of $C(L) - K$ and $v(L) - \sigma L^2$ for varying σ, showing cases with one or three intersections. The parameters are: $\alpha = 1, u_0 = 9.5, \phi = 1, k_d = 0.1, k_l = 0.01, k_r^1 = 0.005, \sigma = 0.2, K = 1, K_S = 0.5, \beta = 1$

4 Periodic dosing

In the previous section, we analyzed the steady-state behavior; however, recent mathematical studies of disinfection argue that periodic dosing might accelerate the removal of the bacteria [6–8]. The structure of this model is more complicated than the well-mixed studies, but more amenable to analysis than the same model in two-dimensions that was introduced in [10]. In this section, we describe the analytic results that have been obtained–that periodic dosing is effective and that the optimal regime depends on the method of dosing. We are able to make predictive bounds on the period of dosing and the corresponding decline of the population. These are complemented with computational exploration of the parameter regime.

4.1 Limit of J, J_L for frequencies $\omega \to \infty$ and $\omega \to 0_+$

Let u be a positive, periodic, piecewise continuous function with period 1. For any $\omega > 0$ we introduce the function

$$u^\omega(t) = u(\omega t), \quad t \in R. \tag{42}$$

Since u^ω is a periodic function with period $P = 1/\omega$, hence, ω is its frequency. Denote by $A^\omega, C^\omega, B_s^\omega, B_{sd}^\omega, B_p^\omega, v^\omega, L^\omega$ the corresponding periodic solutions of the system (4)-(10) on the interval $[0, 1]$. We denote the values of the corresponding functionals by J^ω and J_L^ω, respectively. Now, let μ be the Lebesgue measure of the set $\{t \in [0, 1]; u(t) > 0\}$ and hence, $\mu \in (0, 1]$. In the case of on-off dosing, where $u(t)$ is a step function such that $u(t) > 0$ on $[0, \mu]$ and $u(t) = 0$ on $(\mu, 1]$, the parameter μ is the ratio of the dosing time to period. Following [19], we will use the term 'dosing ratio' for μ. Note that $\mu = 1$ corresponds to constant dosing and $\mu = 0$ would correspond to an unrealistic delta distribution-type dosing.

We make statements about the limiting values of the periodic solutions for $\omega \to \infty$ and $\omega \to 0_+$, respectively. We will, however, skip the proofs of these theorems as they are based on similar results in [19]. The proofs are almost identical, the only difference is the presence of an additional equation for C, this however does not change substantially the gist of the argument.

Theorem 4. *Let $u > 0$ on $(0, 1)$ and let $u_0 = \int_0^1 u(t)dt$ be the average value of u over [0,1]. Then any increasing sequence $\omega_1, \omega_2 ...$ such that $\omega_n \to \infty$ has a subsequence $(\omega_{n_i})_{n\in\mathbb{N}}$ satisfying*

$$L^\infty = \lim_{i\to\infty} L^{\omega_{n_i}}(t) \quad \textit{uniformly for all} \quad t > 0, \tag{43}$$

and all functions $A^{\omega_{n_i}}(x,t), C^{\omega_{n_i}}(x,t), B_s^{\omega_{n_i}}(x,t), B_{sd}^{\omega_{n_i}}(x,t), B_p^{\omega_{n_i}}(x,t), v^{\omega_{n_i}}(x,t), L^{\omega_{n_i}}(x,t)$ for $x \in [0, L^\infty)$ and $t > 0$ converge to functions $A^\infty(x), C^\infty(x), B_s^\infty(x), B_{sd}^\infty(x), B_p^\infty(x)$, $v^\infty(x), L^\infty(x)$ that are independent of t. For the function A^∞ the convergence is only in the weak sense, but all other functions converge locally uniformly in x. Moreover, these functions satisfy on $[0, L^\infty]$ the steady-state equations (14)-(19) with boundary condition $A(L^\infty) = u_0$ and with $k_r(A^\infty)$ replaced by $\Theta = \mu k_r^1 + (1 - \mu)k_r^0$.

Remark. In the limiting cases for $\mu \to 0_+$ and $\mu \to 1_-$, the term $\Theta \to k_r^0$ and $\Theta \to k_r^1$, respectively. This means that for $\mu \approx 1$ the reversion from persister to susceptible cells is very slow, but it increases with decreasing μ. We cannot prove that increased reversion increases the steady-state biofilm thickness L, but numerical simulations indicate that this is the case. In fact, for small periods on-off dosing will be somewhat worse than constant dosing, although the differences are not significant.

Theorem 5. *Let $u(t)$ be a piecewise periodic function of period 1 and consider as in (42) the functions u^ω of period $1/\omega$ and their corresponding periodic solutions $A^\omega, C^\omega, B_s^\omega, B_{sd}^\omega, B_p^\omega$, v^ω, L^ω of the system (4)-(10) on the interval $[0,1]$. Assume that for each $u_0 \in \{u(t); t \in \mathbb{R}\}$ there is a unique nonzero continuous steady-state solution with boundary condition $A(L) = u_0$. Let $J(u_0), J_L(u_0)$ be the values of the two functionals (13) for this steady-state solution. Then*

$$\lim_{\omega\to 0_+} J^\omega = \lim_{\omega\to 0_+} \omega \int_0^{1/\omega} \int_0^{L^\omega(t)} B_s^\omega(x,t) + B_p^\omega(x,t) dx dt = \int_0^1 J(u(t))dt,$$

$$\lim_{\omega\to 0_+} J_L^\omega = \lim_{\omega\to 0_+} \omega \int_0^{1/\omega} L^\omega(t)dt = \int_0^1 J_L(u(t))dt. \tag{44}$$

In case of on-off dosing with $u(t) = u_0/\mu$ on $[0,\mu]$ and $u(t) = 0$ on $(\mu, 1]$, (44) simplifies to

$$\lim_{\omega\to 0_+} J^\omega = \mu J(u_0/\mu) + (1-\mu)J(0), \quad \lim_{\omega\to 0_+} J_L^\omega = \mu J_L(u_0/\mu) + (1-\mu)J_L(0). \tag{45}$$

Remark. In the limiting cases for $\mu \to 0_+$ and $\mu \to 1_-$, the term $\mu J(u_0/\mu) + (1-\mu)J(0) \to J(0)$ and $J(u_0)$, respectively. This suggests that for large periods it is better to have long dosing ratios μ than short ones; this is also demonstrated by numerical results shown below (Figure 5). In the case of unlimited substrate $J(0)$ and $J_L(0)$ can be calculated explicitly and equal to $J(0) = J_L(0) = \frac{\alpha B_s}{\sigma}$, where $B_s = \frac{\alpha(1-k_l)-k_r^0+\sqrt{D}}{2\alpha}$ and $D = (\alpha(1-k_l) - k_r^0)^2 + 4\alpha k_r^0$.

It follows from Theorem 5 that in the limit $\omega \to 0_+$, it is the concavity/convexity of the function $J(u)$ which determines whether or not periodic dosing is better than constant dosing.

Corollary 1. *Let $J(u)$ be the value of the functional (13) for the steady-state solution with constant dose u. Assume that J is a concave down function on the interval $[A_1, A_2]$ and $u(t) \in [A_1, A_2]$. Then*

$$\lim_{\omega\to 0_+} J_\omega = \int_0^1 J(u(t))dt < J(u_0),$$

i.e., for sufficiently small frequencies ω periodic dosing is more effective than constant dosing with dose u_0. Conversely, if J is concave up on the interval $[A_1, A_2]$ and $u(t) \in [A_1, A_2]$, then for sufficiently small frequencies ω, periodic dosing is less effective than constant dosing with dose u_0. In particular, if $J(u) > 0$ for all u, then J is a concave up function for sufficiently large values of u_0; hence, periodic dosing for large doses and small frequencies is less effective than constant dosing. Similar claim holds for the functional J_L.

More explicit results can be obtained in the case of saturation. As in [19], it can be shown that for $u_0 > 0$ sufficiently small on-off dosing with average dose u_0 is better than constant dosing with dose u_0. We remark here that the results in Sections 3 and 4 could be reformulated and extended to the case when the disinfection term $k_d A$ in Equations (6)-(7) is replaced by a nonlinear function $\Phi(A)$ with at most polynomial growth. However, since the numerical results in Section 4.2 for nonlinear disinfection did not yield to substantial differences between the linear and nonlinear case, we will focus on the linear case $k_d A$.

4.2 Computational Studies

In this section we consider numerical approximations to the system of equations (4)-(10) during periodic disinfection. The main goals for the computational studies are to determine how successful disinfection depends on several parameters of the system. It has already been demonstrated ([6, 8]) that success depends on the ratio of dose time to withdrawal time. In [10] the time scale for success as well as the spatial dynamics of the bacteria was setting was investigated. There has been little investigation into other parameter dependence. Here we will vary the period of disinfection, P; the dosing ratio, μ; the disinfectant concentration, u_0.

The last deserves a bit of attention since other studies have assumed that disinfectant was applied at a uniform concentration for a fixed duration. The duration was varied while the concentration was held constant. In this investigation, we also consider the case where the *total* biocide is fixed and vary the rate of application of the biocide. This follows the methods introduced in [18, 20]. We use the term *constant average* to refer to application of a constant biocide concentration for a period of time and *constant total* to refer to the second protocol. The numerical simulations are based on the method of characteristics and use a second-order explicit Runge-Kutte method [19], however, to account for the presence of substrate, Newton's method has been applied.

Throughout this section, we will use two methods to consider successful disinfection and optimal disinfection. The first connects the the theorems in the previous section, namely how well does periodic dosing compare with constant dosing and was used in [18,20].The functional $J(\mu, P)$ describes the average concentration of bacteria as the length of periodic disinfection goes to infinity. Minima of J indicate optimal regimes since the total bacterial concentration is the smallest. The ratio of $J(\mu, P)$ to constant dosing, $J(\mu = 1, P)$ determines whether periodic disinfection is better or worse than constant dosing. This compares well with the theorems described in the previous section.

The second method is to calculate the *survival curves* similar to curves developed in [6]. For fixed parameters the total bacterial concentration, $\int_0^{L(t)} B_s + B_p \, dx \, dt$, is a function of time. Clearly this must tend to zero if the disinfection cycle is successful. By comparing survival curves for different parameters, we get a different view of success/failure of disinfection and can compare the effectiveness of different disinfection protocols.

Study 1: Constant Average

Similar to [18, 20], we vary the fraction of the period corresponding to antibiotic application. That is we let $u(t)$ be a piecewise constant function that is positive on the interval $(0, \mu P)$ and zero on $(\mu P, P)$. We then vary μ and P while other parameters are

shown in Table 1. The surface shown in the left panel of Figure 5 is $J(\mu, P)/J(1, P)$ and compares the values of J with varying fractional time to that of constant dosing for each fixed period. We see that the top left (small fraction of application and large period) corresponds to protocols that are unsuccessful. For large enough fraction of application we have successful treatment and for a given P the optimal protocol is periodic dosing rather than constant dosing.

We also compare results of two different simulations in the right panel of Figure 5. As the period of application becomes longer while the fraction is fixed, the window of optimal treatment changes. This is qualitatively different from the next set of simulations. We note that there is actually more biocide being used in the unsuccessful treatment since $u_0 \times 40 \times 0.2 > u_0 \times 20 \times 0.2$. Thus it is the disinfection regime rather than amount of biocide that distinguishes the success/failure.

Study II: Constant Total

In this study, we fix the total amount of disinfectant that can be applied, which is more compatible with clinic applications where it is not possible to maintain a constant source of antibiotic (e.g. within the blood stream). The amount of antibiotic in the

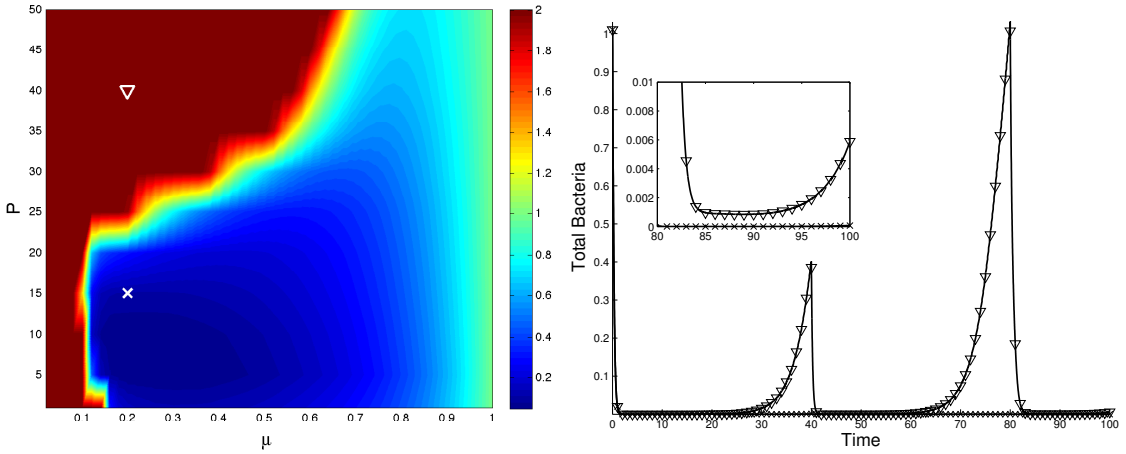

(a) (b)

Figure 5: (a) The surface $J(\mu, P)$ for disinfection with constant antibiotic applied for a fraction, μ of a period, P. The upper region corresponds to unsuccessful treatment. As the dosing period becomes larger, the region for successful disinfection becomes smaller. The markers indicate parameter pairs used to compare survival curves in the right panel. (b): A comparison of survival curves for varying periods. These two parameter pairs were chosen to be representative of the effect of varying the period for fixed fractional length. The symbols correspond to the left panel ($\mu = 0.20$): The symbol x corresponds to $P = 20$, triangle corresponds to $P = 40$. The inset curves are the las 20 time steps of the same data with a different scale to emphasize the difference between the two parameter sets at the end of the simulation. Parameters are given in Table I.

system is therefore related to the fraction of the period where the antibiotic is applied, $u_0 = \frac{\hat{u}}{\mu}$. For small fractions (i.e. short application cycle relative to the period) the biocide concentration that is applied is large. In Figure 6, we show the surface, J (left panel), and several survival curves for fixed values of μ and P (right panel). We see that there is a window where periodic disinfection is more successful than constant dosing. However, as the period increases, too small a fraction is not successful at all (upper left corner in 6.

We see that there are regions where constant dosing is more effective than periodic dosing; however, the optimal choice occurs in a central band of parameters. Therefore the optimal timing depends on the period and application fractional period. This has particular implications for treatment. For biocides that have side effects that occur only for high concentrations, it is better to extend the period so that the application can be spread out further. This may explain why the periodic treatment in [24] was ineffective.

Study III: Varying Growth Rates

In this section, we consider the effect of varying the growth rate of the bacteria on survival using constant total application in this set. Very small μ is rapid application of high concentration of antibiotic. The previous simulations indicate that the time the

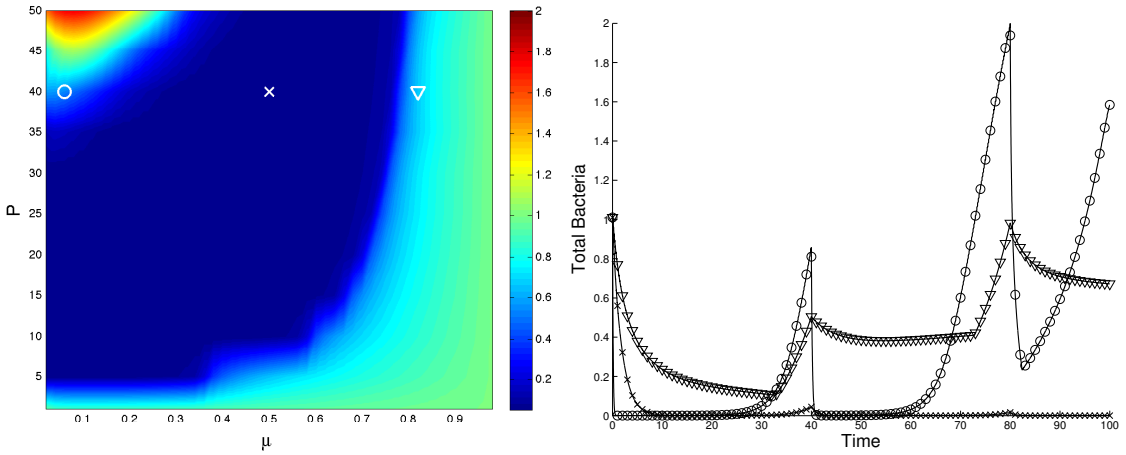

(a) (b)

Figure 6: (a): The surface $J(\mu, P)$ for disinfection where the total biocide that is applied is held constant as the fractional application time and period are varied. The central band of dark blue corresponds to optimal treatments. The markers indicate parameter pairs used to compare survival curves in the right panel.
(b): A comparison of survival curves for varying fractions. These three parameter pairs were chosen to be representative of an optimal protocol with a moderate fraction μ. The symbols correspond to the left panel ($P = 40$): The symbol circle corresponds to $\mu = 0.06$, the symbol x corresponds to $\mu = 0.5$ and the triangle symbol corresponds to $\mu = 0.82$. We see that parameters in the blue region are successful while the others are unsuccessful. Parameters are given in Table I.

population has to recover from an antibiotic challenge is one of the key factors in success or failure. If the bacteria that revert from persister have ample time to replace the killed bacteria, the treatment will be unsuccessful. This means that if the bacteria grow faster, it will alter the distribution of success and failure. Figure 7 shows the surface $J(\mu, \alpha)$ (left panel) indicating that as the growth rate increases, the window of success shrinks. In fact, for slow growth, instantaneous application is the best course. The same figure (right panel) compares the survival curves again indicating that the optimal is in fact successful. The key results here is that the withdrawal time should be measured relative to the potential growth for reproducing bacteria and, therefore, the nutrient regime may also play a more complicated role in disinfection.

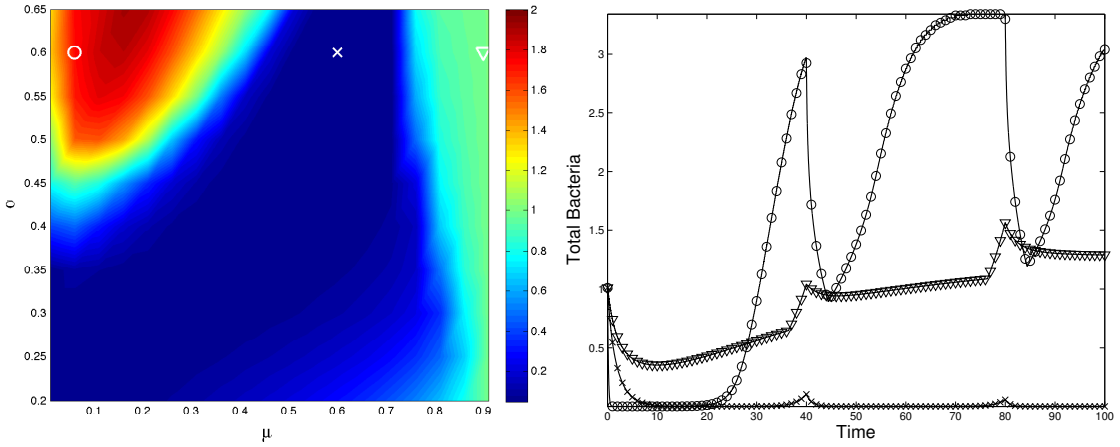

(a) (b)

Figure 7: (a): The surface $J(\mu, \alpha)$ showing the narrowing window of successful treatment as the growth rate increases. The survival curves at particular parameter pairs are shown in the right panel.
(b): A comparison of survival curves for varying fractions and fixed growth rate. These three parameter pairs were chosen to be representative of an optimal protocol with a moderate fraction μ. The symbols correspond to the left panel ($\alpha = 0.6$): The circle corresponds to $\mu = 0.06$, the x corresponds to $\mu = 0.6$ and the triangle corresponds to $\mu = 0.9$. We see that parameters in the blue region are successful while the others are unsuccessful. Parameters are given in Table I except that α now varies between 0.2 and 0.65.

5 Summary

This manuscript deals with the important question of removal of bacteria bound within a biofilm matrix. We take into account both susceptible bacteria and a small subpopulation of tolerant bacteria. Evidence of persister subpopulations has been accumulating recently; however, there is still quite a bit that is not understood. Furthermore, the implications of persister dynamics is not yet well described. In this manuscript, the dynamics between the two populations incorporates current hypotheses of persisters. Namely, that susceptible bacteria can convert to persisters at a rate that depends on the nutrient level (i.e. the growth stage). Persister reversion to susceptibles occurs at a slower rate and is inhibited by the presence of an antibiotic. Disinfection depends on the growth rate, which means that the biofilm structure and subsequent nutrient gradients has a profound affect on the disinfection. The main motivation for this study is to couple analytic and computational studies of the impact of persister dynamics on disinfection of bacterial biofilms, especially in the case of periodic disinfection.

In Theorem 3 we give sufficient conditions for the existence of trivial/nontrivial steady states and show numerically that non-unique steady-states can occur, which seem to depend on the rate of detachment (Figure 4). Moreover, a sufficiently large initial antibiotic dose can influence dosing efficacy, since the time dependent solutions may converge to a steady-state with smaller biofilm thickness (Figure 3). In Theorems 4-5 the limiting behavior of periodic solutions for small and large periods has been summarized, which allows us to compare the analytical results with simulations. For large periods, longer dosing time is more effective than short one (as shown also in Figure 5) and, for very small periods, reversion from persister to susceptible cells decreases with increasing dosing time. In the latter case numerical examples suggest that on-off dosing becomes worse than constant dosing, thought the differences are negligible. As a consequence of Theorem 5 we also provide sufficient conditions under which period dosing is better or worse than constant dosing. The presence of substrate in the model does not allow us to obtain such explicit results for periodic dosing as in [19]. For example, we can only state under the assumption of saturation in the persister model that for small doses of antibiotics, on-off dosing is always more effective than constant dosing. Hence, detailed computational studies of the model are necessary.

The particular simulations that we have presented explore the role of the period and dose ratio for different dosing methods (e.g. constant total and constant average) and growth rates. The main observation is that periodic dosing may be the optimal method, but ensuring that it is requires determining the dose ratio for a given period. In general, for intermediate periods and intermediate dose ratios, periodic disinfection is more effective than constant dosing. The extends observations mode in previous studies ([6–8] to explore the role of the period more fully. As the period becomes longer, all our simulations indicate that the window of success becomes narrower. Moreover, the simulation in Study III indicates that the window is larger if the bacteria are growing more rapidly. This is because the important processes–disinfection and persister reversion– depend on the growth rate. As these become larger, it is easier to eliminate the biofilm. We emphasize that although we have estimated our specific parameters, the analysis in the preceding sections indicate that the general behavior is quite robust.

There are several novel aspects of this study including robust biofilm dynamics and

analysis in one-dimension. Previous models either neglect the spatial aspect of the biofilm or study the model in two-dimensions only computationally. Using methods similar to those used to analyze an adaptive response, we are able to prove the existence and stability of the steady-state system and predict the optimal dosing period. One of the most useful aspects of the analytic studies is that the qualitative results do not depend strongly on the forms of the transition rates. Although the forms of f and g have been specified for the quantitative numerical studies, the theorems carry over for a wide variety of functional dependencies. Because there is some debate about the mechanisms of persister formation [28,29], it is not clear whether the quantitative predictions are correct; however, it is quite reasonable to conclude that the qualitative results are valid.

A second extension that is developed in this study has to to with the interplay between the period and optimal fraction of the period for disinfection. The computational studies indicate that there is a complicated relationship that is due primarily to the interplay between the reversion of persisters and the presence of the antibiotic. Because the time scale of disinfection is quite long (perhaps not infinite, but certainly longer than optimal), it seems that the bacteria can be prevented from reverting back to susceptible phenotype if the antibiotic is present. Additionally, the reversion rate has been demonstrated to be much slower than other phenotypic transitions. Therefore, it is crucial that the off period is long enough to allow much of the persister population to revert. This is evident in the two-dimensional plots of the surface J. We find that, when the average disinfectant applied during the on-period is held constant, the region for successful disinfection becomes smaller as the period increases. Similarly, if the disinfection concentration during the on-period is held constant, there is a window of successful disinfection. This has consequences in clinical settings and the design of drug delivery devices and protocols. Clearly, the quantitative predictions in this manuscript might be incorrect but we argue that the generality of the qualitative results argue for more investigation into the processes so that more accurate predictions can be derived.

6 Acknowledgements

NC was supported by by NSF DMS-1122378.

Parameter	Notation	Value
Substrate Utilization	$f(C)$	$\frac{\beta C}{C+K_S}$
Growth Function	$g(C)$	$\frac{\alpha C}{C+K_S}$
Maximal Consumption Rate	β	2.08
Maximal Growth Rate	α	0.417
Disinfection Scale	k_d	0.1
Loss Scale	k_l	0.001
Reversion Scale	k_r	0.05
Thiele Modulus	ϕ_a	1.0
Detachement Rate	σ	0.01

Table 1: Model notation and parameters for the simulations of the solutions to Equations 4-10.

References

[1] J. W. Costerton, Z Lewandowski, D E Caldwell, D R Korber, and H M Lappin-Scott. Microbial biofilms. *Annual Review of Microbiology*, 49:711–745, 1995.

[2] J W Costerton, K J Cheng, G G Geesey, T I Ladd, J C Nickel, M Dasgupta, and T J Marrie. Bacterial biofilms in nature and disease. *Annual Review of Microbiology*, 41:435–464, 1987.

[3] J. W. Costerton, P. S. Stewart, and E. P. Greenberg. Bacterial biofilms: A common cause of persistent infections. *Science*, 284(5418):1318–1322, 1999.

[4] C. A. Fux, J. W. Costerton, P. S. Stewart, and P. Stoodley. Survival strategies of infectious biofilms. *Trends in Microbiology*, 13(1):34–40, 2005.

[5] David Davies. Understanding biofilm resistance to antibacterial agents. *Nature Reviews Drug Discovery*, 2(2):114–122, February 2003.

[6] N. G. Cogan. *Effects of persister formation on bacterial response to dosing.* Journal of Theoretical Biology, 2005.

[7] N. G. Cogan. Incorporating toxin hypothesis into a mathematical model of persister formation and dynamics. *Journal of Theoretical Biology*, 248:340–349, 2007.

[8] P. De Leenheer and N. Cogan. Failure of antibiotic treatment in microbial populations, j. *Math. Biol.*, 59:563–579, 2009.

[9] N. G. Cogan, Ricardo Cortez, and Lisa J. Fauci. Modeling physiological resistence in bacterial biofilms. *Bulletin of Mathematical Biology*, 67(4):831–853, 2005.

[10] N. G. Cogan. An extension of the boundary integral method applied to periodic disinfection of a dynamic biofilm. *SIAM Journal on Applied Mathematics*, 70(7):2281–2307, 2010.

[11] Nasim Muhammad and Hermann J. Eberl model parameter uncertainties in a dual-species biofilm competition model affect ecological output parameters much stronger than morphological ones. *Mathematical Biosciences*, 233(1):1–18, 2011.

[12] P. S. Stewart. Diffusion in biofilms. *J. Bacteriol*, 185(5):1485–1491, 2003.

[13] P. S. Stewart. Theorethical aspects of antimicobial diffusion into microbial biofilms. *Antimicrobial Agents and Chemotheraphy*, 40(11):2517–2522, 1996.

[14] P. S. Stewart, W. M. Davison, and J. N. Steenbergen. Daptomycin rapidly penetrates a staphylococcus epidermidis biofilm, antimicrob. *Agents Chemother*, 53(8):3505–3507, 2009.

[15] E. Tuomanen, R. Cozens, W. Tosch, O. Zak, and A. Tomasz. Rate of killing of escherichia coli by β-lactam antibiotics is strictly proportional to the rate of bacterial growth. *Journal of General Microbiology*, 132:1297–1304, 1986.

[16] Karen D. Xu, Gordon A. McFeters, and Philip S. Stewart. Biofilm resistance to antimicrobial agents. *Microbiology*, 146:547–549, 2000.

[17] Philip S Stewart and J William Costerton. Antibiotic resistance of bacteria in biofilms. *The Lancet*, 358(9276):135–138, 2001.

[18] B. Szomolay, I. Klapper, J. Dockery, and P. S. Stewart. Adaptive responses to antimicrobial agents in biofilms. *Environmental Microbiology*, 7(8):1186–1191, 2005.

[19] B. Szomolay, I. Klapper, and M. Dindos. Analysis of adaptive response to dosing protocols for biofilm control. *SIAM Appl Math*, 70:3175–3202, 2010.

[20] B. Szomolay. Analysis of a moving boundary value problem arising in biofilm modeling, math. *Meth. Appl. Sc.*, 31:1835–1859, 2008.

[21] Kim Lewis. Riddle of biofilm resistance. *Antimicrobial Agents and Chemotherapy*, 45(4):999–1007, April 2001.

[22] Iris Keren, Niilo Kaldalu, Amy Spoering, Yipeng Wang, and Kim Lewis. Persister cells and tolerance to antimicrobials. *FEMS Microbiology Letters*, 230:13–18, 2004.

[23] M. Desai, T. Buhler, P. H. Weller, and M. R. W. Brown. Increasing resistance of planktonic and biofilm cultures of *Burkholderia cepecia* to ciproflaxacin and ceftazidime during exponential growth. *Journal of Antimicrobial Chemotherapy*, 42:153–160, 1998.

[24] Lawrence R. Mulcahy, Jane L. Burns, Stephen Lory, and Kim Lewis. Emergence of *pseudomonas aeruginosa* strains producing high levels of persister cells in patients with cystic fibrosis. *J. Bacteriol*, 192(23):6191–6199, 2010.

[25] N. G. Cogan and R. D. Guy. Multiphase flow models of biogels from crawling cells to bacterial biofilms. *HFSP J*, 4:11–25, 2010.

[26] P. S. Stewart. A model of biofilm detachment. *Biotechnology and Bioengineering*, 41:111–117, 1993.

[27] R. Kommedal and R. Bakke. Modeling *Pseudomonas aeruginosa* biofilm detachment. *HIT Working Paper*, 3, 2003.

[28] N. W. Balaban, J. Merrin Q., R. Chait, L. Kowalik, and S. Leibler. Persistence as a phenotypic switch. *Science*, 305:1622–1625, 2005.

[29] G. L. Drusano, N. Sgambati, A. Eichas, D. Brown, R. Kulawy, and A Louie. The combination of rifampin plus moxifloxacin is synergistic for suppression of resistance but antagonistic for cell kill of *Mycobacterium tuberculosis* as determined in a hollow-fiber infection model. *Mbio*, 1(10):139–10, 2010.